Deposition of Ni nanoparticles onto porous supports using supercritical CO_2: effect of the precursor and reduction methodology

Jacobo Morère, Sergio Royuela, Guillermo Asensio, Pablo Palomino, Eduardo Enciso, Concepción Pando and Albertina Cabañas*

Department of Physical-Chemistry I, Universidad Complutense, Ciudad Universitaria s/n, 28040 Madrid, Spain

Keywords: Metal deposition, Nickel nanoparticles, Supercritical CO_2, Mesoporous SiO_2 SBA-15, Mesoporous Carbon

Summary

The deposition of Ni nanoparticles into porous supports is very important in catalysis. In this paper, we explore the use of supercritical CO_2 ($scCO_2$) as a green solvent to deposit Ni nanoparticles on mesoporous SiO_2 SBA-15 and a carbon xerogel. The good transport properties of $scCO_2$ allowed the efficient penetration of metal precursors dissolved in $scCO_2$ within the pores of the support without damaging its structure. Nickel hexafluoroacetylacetonate hydrate $[Ni(hfac)_2 \cdot 2H_2O]$, nickel acetylacetonate $[Ni(acac)_2]$, bis(cyclopentadienyl)nickel $[Ni(Cp)_2]$, $Ni(NO_3)_2 \cdot 6H_2O$ and $NiCl_2 \cdot 6H_2O$ were tried as precursors. Different methodologies were used: impregnation in $scCO_2$ and reduction in H_2/N_2 at 400 ºC and low pressure, reactive deposition using H_2 at 200-250 ºC in $scCO_2$ and reactive deposition using EtOH at 150-200 ºC in $scCO_2$. The effect of precursor and methodology on the nickel particle size and the material homogeneity (on the different substrates) was analyzed. This technology offers many opportunities in the preparation of metal-nanostructured materials.

Main Text

1. Introduction

Ni nanostructured materials have many applications in catalysis and microelectronics. Ni films deposited on SiO_2 wafers are used in data storage [1] and in giant magnetoresistance devices [2]. On the other hand, Ni supported nanoparticles have been used as catalyst in hydrogenation reactions [3], hydrocarbon reforming [4] or methane cracking [5]. Ni nanoparticles may be also used as catalyst to grow carbon nanotubes [6] or as sensors, for example in the determination of uric acid [7]. In comparison to noble metals such as Pt and Pd, Ni is much cheaper and abundant, and it is a very versatile catalyst for different chemical reactions.

Metal nanoparticles exhibit very interesting properties in comparison to their bulk counterparts [8-10]. Apart from their significantly higher surface to volume ratio, they have reduced cohesive energy which turns the surface atoms very reactive. Furthermore electronic, optical and magnetic properties of the metal nanoparticles change dramatically and become surface, shape and size-dependent, offering many opportunities in catalysis, electronics, information storage, photonics, sensing, imaging, and medicine (drug delivery and contrast agents) [11-14].

Nanoparticles tend however to aggregate and in most applications need to be stabilised. One approach is to include the metal nanoparticles into a porous support, inorganic or polymeric, which stabilises the particles by inhibiting the particle growth and avoiding their aggregation while preserving the properties of the metal nanoparticles. In this case, the nanoparticles create active sites on the support and the composite material may exhibit improved properties in comparison to the porous support and the nanoparticles by themselves. Furthermore, it facilitates handling. The synthesis of supported metal nanoparticles on solid porous supports and the different preparations routes have been recently reviewed [12].

The use of supercritical fluids and in particular supercritical CO_2 ($scCO_2$) in the synthesis of metal nanostructured

*Author for correspondence (a.cabanas@quim.ucm.es).

materials offers real advantages over other more conventional techniques. $scCO_2$ is considered a green solvent [15] because it is nontoxic, nonflammable, and has a moderate critical temperature and pressure (Tc = 304.15 K, Pc = 7.38 MPa) [16]. Furthermore, it is a gas at ambient pressure and can be completely released by decreasing pressure, does not leave any residue and can be recycled. Most of the CO_2 used nowadays in the laboratory and industry is obtained as a sub-product in industrial processes such as the ammonia synthesis.

Prof. Sir Martyn Poliakoff has devoted much of his career to promote the use of supercritical fluids as green solvents for green chemistry. He envisions that high pressure CO_2 obtained directly from carbon capture and storage processes may become a commodity, stimulating the use of $scCO_2$ in many different processes and bringing the supercritical technology much closer to commercial-scale [17, 18].

The advantages of using $scCO_2$ in materials synthesis go beyond those related to its green nature [19]. In particular, the favorable transport properties: low viscosity, high diffusivity and very low surface tension, along with its solvating power, allow the efficient penetration of precursors into porous materials and fragile matrixes [20]. In this way, precursors can be introduced within the micro and mesopores of different materials without damaging their pore structure during depressurization, as capillary forces are avoided. On the other hand, the high compressibility of $scCO_2$ makes it possible to tune their properties from gas-like to liquid-like, which gives an extra degree of control in the synthesis. Furthermore, in some cases, the temperature and reaction time of the process can be reduced [21, 22].

The Supercritical Fluid Deposition (SCFD) technique has been used to deposit metal or metal oxides of different morphology into organic and inorganic substrates [23, 24]. The method involves the dissolution of a metal precursor in $scCO_2$ and its adsorption onto the support. The precursor adsorption depends on the precursor-CO_2-substrate interaction and it varies with pressure and temperature [25]. The metal precursor adsorbed is then chemically or thermally decomposed. The decomposition can be carried out after the depressurization or at supercritical conditions. Different decomposition methods are used: impregnation in $scCO_2$ and further reduction in N_2/H_2 at high temperature/low pressure, chemical reduction using H_2 in $scCO_2$, chemical reduction using EtOH in $scCO_2$ and thermal decomposition in $scCO_2$. Depending on the experimental conditions, metal nanoparticles, nanowires or continuous supported films can be produced. Using this technique, we have previously deposited Pd and Ru nanoparticles into mesoporous supports [25-27]. The materials were very homogeneous and performed as efficient catalysts in different hydrogenation reactions.

The SCFD of Ni-nanostructured materials has been attempted a few times. In most experiments, nickel bis(cyclopentadienyl) [$Ni(Cp)_2$] has been chemically reduced using H_2 in $scCO_2$. This precursor exhibits a high solubility in $scCO_2$ [28, 29] but it is air and light sensitive. Blackburn et al.[1] produced continuous Ni films on planar and patterned silicon wafers. The deposition was performed at 60ºC and 20 MPa on Pd seeded wafers. Increasing the temperature to 120ºC, the deposition proceeded without the use of the Pd catalyst on bare silicon wafers. Hunde et al. [2] prepared Ni films on silicon and TaN and TiN wafers at higher temperatures 175-200ºC and pressures 19-23 MPa. Peng et al. [30] deposited Ni nanoparticles on multi wall carbon nanotubes (MWCNT) and Ni films on planar SiO_2 and Al_2O_3 surfaces. Deposition of Ni nanoparticles on MWCNT was carried out at 70ºC and 17 MPa after 7-8 hours. The authors suggest that Ni metal deposition proceeded through nucleation on chemically active defects on the MWCNT. Such a low deposition temperature might indicate the presence of metal residues in the MWCNT acting as catalytic sites. Finally, Bozbag et al. [31] have deposited Ni nanoparticles and nanowires on carbon aerogels from nickel acetylacetonate [$Ni(acac)_2$]. Although the solubility of this precursor in $scCO_2$ is very low [28], carbon aerogels were successfully impregnated with this precursor at 60ºC and 30 MPa in $scCO_2$ for 24 hours followed by reduction at low pressure and 500ºC in N_2 or 170 ºC in H_2. In both cases, Ni nanoparticles were formed. When the reduction in H_2 was performed at 200 ºC, Ni nanowires were obtained on the surface of the carbon aerogels.

On the other hand, metal nitrates in CO_2-expanded ethanol solutions have been used by B.X. Han and coworkers [32-34] to deposit different metal and metal oxides on carbon nanotubes. Following this approach, Ming et al. [35] have decomposed inorganic salts such as $Ni(NO_3)_2 \cdot 6H_2O$ at 200ºC in CO_2-expanded ethanol solutions. From the decompositions of these salts, Ni oligomers are obtained. By further increasing the temperature, it is expected that Ni nanoparticles could be obtained.

In this paper, the use of different Ni precursors and decomposition methodologies in the deposition of Ni nanostructures on mesoporous materials is explored. The aim of the study is to relate these variables with the morphology and structure of the final metal-composite material and to establish the best conditions to deposit Ni nanoparticles homogeneously distributed on high surface area supports. These metal-composite materials may exhibit very interesting catalytic properties.

2. Experimental details

(a) Materials and supports

Tetraethylorthosilicate (TEOS, 99% pure) and poly(ethylene glycol)-block-poly(propylene glycol)-block-poly(ethylene glycol) (Mw=5800) (PEO-PPO-PEO) were obtained from Sigma-Aldrich. Carbon xerogels were prepared from resorcinol (99% pure) and sodium hydroxide pellets obtained from Sigma Aldrich and formaldehyde (37% in water) from Panreac. The precursors nickel hexafluoroacetylacetonate hydrate ($Ni(hfac)_2 \cdot 2H_2O$, 98% pure), nickel acetylacetonate ($Ni(acac)_2$, 95% pure), bis(cyclopentadienyl)nickel ($Ni(Cp)_2$, 98% pure), $Ni(NO_3)_2 \cdot 6H_2O$ (98.5% pure) and $NiCl_2 \cdot 6H_2O$ (99.999% pure) were obtained from Sigma-Aldrich. All chemicals were used as received. $Ni(Cp)_2$ was kept in a dry box and

protected from the light. CO_2 (purity >99.99%) and H_2 (purity >99.999%) were supplied by Air Liquide. 5% H_2/N_2 forming gas was supplied by Contse.

Hydrophilic silica SBA-15 and a hydrophobic carbon xerogel were used as supports. Both materials exhibit high surface area and pore sizes in the mesopore range which facilitate the transport of large molecules. SiO_2 SBA-15 has a very well defined pore structure of interconnected cylindrical mesopores and was chosen as a model support. Mesoporous carbon xerogels exhibit both mesoporosity and microporosity and are currently used as catalyst supports.

Mesoporous silica SBA-15 was prepared following the procedure described by Zhao *et al.*[36, 37]. In a typical experiment, 4.0 g of PEO-PPO-PEO were dissolved in 30 g of water and 120 g of 2 M HCl solution with stirring at 35 ºC. Then 8.5 g of TEOS was added into the solution with stirring at 40ºC for 20 hours. The mixture was aged at 100ºC without stirring for a further 12 hours. The solid residue was filtered, washed with ethanol several times and calcined in air at 550 ºC for 6 hours. Heating rate from room temperature was 1ºC/min.

Mesoporous carbon xerogels were prepared following a similar procedure to that described in the literature [38] with some modifications. Briefly, resorcinol (R) and formaldehyde were mixed with deonized water (W) maintaining always a molar ratio R/W of 0.04. Then, a sodium hydroxide solution was added as catalyst until the pH reached a value of 6.55. The mixture was stirred, sealed and introduced in an oven at 80 ºC. After three days, the wet xerogel was dried in air at 80 ºC during 48 hours. The resulting dry xerogel was then pyrolysed in N_2 atmosphere at 900 ºC (temperature ramp used: 3ºC min^{-1}) during 4 hours to produce the carbon xerogel. By careful control of the reaction conditions, the micro- and meso-porosity of the carbon xerogels could be finely tuned [39, 40].

(b) Deposition experiments

Ni deposition experiments were carried out in supercritical CO_2 following three different procedures: a) impregnation, b) reactive deposition using H_2 and c) reactive deposition using EtOH. $Ni(hfac)_2 \cdot 2H_2O$, $Ni(acac)_2$, $Ni(Cp)_2$, $Ni(NO_3)_2 \cdot 6H_2O$ and $NiCl_2 \cdot 6H_2O$ were tried as metal precursors. High surface area mesoporous silica SBA-15 and a carbon xerogel were used as supports. These experiments involve high-pressure and/or temperature and they should be only performed with caution using appropriate high-pressure equipment and safety precautions.

Experiments were conducted in a *ca*. 100 mL stirred high-pressure reactor (Autoclave Eng. Inc.) in the batch mode. Support and precursor were loaded into the reactor. Then the reactor was heated by a heating jacket connected to a PDI controller at a temperature between 35 and 80 ºC, depending on the experiment, and was then filled with CO_2 using a high-pressure syringe pump (Isco, Inc. Model 260D) thermostated at the same temperature up to a pressure between 9.0 and 13.5 MPa. The temperature was measured using a K-type thermocouple. The pressure was measured using a pressure gauge. Reactor was stirred at 200 rpm.

In the *impregnation experiments*, reaction conditions were kept for most experiments for 24 hours to allow reaching the adsorption equilibrium. The reactor was then depressurized through a needle valve in 1 hour. The Ni impregnated samples were then decomposed in a tubular furnace in N_2/H_2 for 5 hours at 400 ºC and atmospheric pressure. Heating rate in both cases was 10 ºC/min.

In the *reactive deposition experiments using H_2*, dissolution of the precursor and adsorption on the support in $scCO_2$ was performed for 1-2 hours. Afterwards excess H_2 was added to the reactor using a ca. 30 mL auxiliary cell constructed from Swagelok ¾ inch pipe and filled with 4.0 MPa H_2, by flushing CO_2 from the thermostated Isco high-pressure syringe pump through the auxiliary cell up to a final pressure of 10.0 MPa. At these conditions, reduction of the precursor did not take place. To promote the precursor reduction, the temperature was increased at 150-250 ºC and kept at these conditions for 2 hours. The heater was turned off, and the depressurization was carried out through a needle valve in 1 hour.

In the *reactive deposition experiments using EtOH*, the precursor and a small amount of ethanol were loaded together into the reactor along with the substrate. The reactor was then filled with sCO_2 at 80 ºC and 13.5 MPa to promote dissolution of the precursor in the supercritical mixture and its impregnation on the support for 1-2 hours. In the experiment with $Ni(Cp)_2$, the reactor was loaded at 60ºC and 11.0 MPa. Then the reactor was heated at 150-200 ºC for another 2 hours for its decomposition. During these experiments the pressure was kept below 30.0 MPa (which is the maximum pressure rating of the equipment) by venting a small amount of the CO_2 solution from 100 ºC. Then, the heater was turned off and the reactor was depressurized through a needle valve in 1 hour.

(c) Materials characterization

Materials were characterized using transmission electron microscopy (TEM), X-ray diffraction (XRD), N_2-adsorption and thermogravimetric analysis (TGA). TEM were carried out on a JEOL JEM 2100 electron microscope working at 200 kV and a JEOL-JEM 3000F electron microscope operating at 300 kV. Both TEM microscopes were equipped with a double tilting (±25º) and Energy-dispersive Detection X-ray analysis (EDX) (Oxford INCA). Samples were dispersed in 1-butanol over copper grids and dried in air. Wide angle XRD patterns of the composite materials were collected using a X´PERT MPD diffractometer with Cu K-α radiation on the conventional Bragg-Brentano geometry at 2θ values between 10 and 80º. Porosity of the supports was determined by measuring the N_2 adsorption-desorption isotherms at -196 ºC using a Micromeritics ASAP-2020 instrument. The specific surface area, S_{BET}, was determined by applying the BET model [41] and the pore size distributions were calculated using the Barrett, Joyner and Halenda (BJH) method for a cylindrical pore model corrected by the statistical thickness [42]. TGA of selected samples was obtained on a Perkin-Elmer Pyris 1 at a heating rate of 10 ºC/min in H_2/N_2 flow (100 cm^3/min).

3. Results and discussion

Deposition experiments were performed on mesoporous SiO_2 SBA-15 and a carbon xerogel. Mesoporous SiO_2 SBA-15 is a hydrophilic porous support composed of a hexagonal array of one-dimensional cylindrical mesopores. In contrast to MCM-41 materials, mesopores in SBA-15 are interconnected through small micro and mesopores due to the polyethyleneoxide blocks (PEO) in the triblock copolymer [43, 44]. S_{BET} for the SiO_2 supports was ca. 560-580 m^2/g and pore size is 5.6-5.9 nm (depending on the sample). The mesoporous carbon xerogel (C14) used in these experiments is a hydrophobic support with S_{BET} equal to 650 m^2/g and a mesopore size of 14 nm.

A summary of the deposition experiments is given in Table 1 showing the impregnation and reduction conditions, the EtOH mol percentage in CO_2, the maximum Ni loading based on the initial quantities of Ni precursor and SiO_2 and the Ni percentage estimated from EDX analysis of the Ni/SiO_2 samples (average of several samples). Quantification by EDX was not performed on the Ni/C14 samples, due to the low sensitivity of the technique to lighter elements. Particle size/morphology is based on the TEM images. Experiments are discussed for the different methodologies. For most experiments the mass of the support was 50-150 mg and that of the precursor 35-75 mg, and the maximum loading was ca. 30% wt. Experiments with the inorganic salts were performed using ca. 0.5 g of precursor for ca. 90% wt. loadings. Impregnation experiments with $Ni(Cp)_2$ were also conducted at higher loadings. These large loading were used to favour incorporation of the metal in the support.

(a) Ni composite materials obtained by reactive deposition using H_2

Reactive deposition experiments were performed using $Ni(Cp)_2$. In these experiments, the impregnation step was carried out at 60 ºC and 11.0 or 9.5 MPa and the H_2 reduction was performed at 200 and 250 ºC. Loading pressure was varied to avoid exceeding the pressure rate of the reactor during heating. The mole fraction solubility of $Ni(Cp)_2$ in $scCO_2$ at 60 ºC and 15.0 MPa is $y = 1.42\ 10^{-3}$ [28, 29] and, at the loading conditions, the precursor was completely soluble in the supercritical phase. Ni deposition proceeded readily on SiO_2 SBA-15 and the carbon xerogel C14 from 150 ºC.

Figure 1 shows wide angle XRD data for the samples prepared on SiO_2 and C14 at 150 ºC, showing reflexions at 2 theta values equal to 44.5, 51.8 and 76.3º which correspond to the Ni cubic phase [PDF-040850]. The broad reflection at 2θ ca. 22º is due to the amorphous support: either SiO_2 or carbon (very weak). Metal reflexions are broader in the sample deposited on carbon.

Figure 2 shows TEM images of the Ni/SiO_2 samples obtained at 200 ºC (Fig. 2 a,b) an 250ºC (Fig. 2 c,d). Images show the mesoporous channels of the SiO_2 SBA-15 and dark Ni particles deposited on the support. Some of the nanoparticles are very small and seem to be deposited within the SiO_2 mesopores. Particle size is limited by the pore diameter of the support (in this case ca. 6 nm). Additionally, larger Ni particles 20-30 nm in size are also deposited on the external surface of the material. EDX analysis of this sample showed large variations of the Ni content depending on the region, and reached values of 13% Ni mol in some regions for the sample deposited at 200 ºC. The Ni content was lower in other regions. EDX analysis of the samples prepared at 250 ºC gave average values close to 4% mol. The large uncertainty on the Ni content of the sample is most likely due to the presence of these large particles.

To confirm that nanoparticles were deposited within the mesopores, the sample prepared at 200 ºC was further heated in air at 400 ºC for 5 hour. XRD of the calcined sample is also show in Figure 1 and shows new peaks at ca. 37.0, 43.5 and 62.5º that can be assigned to NiO [PDF-441159].Weak peaks of Ni are still present, which indicates that most Ni nanoparticles have been oxidized. Peaks for NiO are quite broad.

TEM images of the calcined sample are also shown in Figure 2 (e,f). In comparison to the sample before the thermal treatment (a,b), the number of large particles on the external surface has decreased. Furthermore, very large and isolated particles were also observed in the calcined sample (images not shown here). The large particles on the external surface of the support aggregate during the thermal treatment, whilst the small particles within the mesopores do not suffer much aggregation with the thermal treatment.

Figure 3 shows TEM images of the sample deposited on the carbon xerogel C14. Images show Ni nanoparticles uniformly distributed throughout the support with sizes ranging from 10-25 nm. Analysis by the Scherrer equation of the mean particle size from the peak at 44.5º, gave and average size of ca. 14-15 nm. The average particle size is close to the mesopore size of the support and suggests that the pore size limits the crystal growth. Fit of the XRD peak was however not very good, suggesting the presence of a bimodal particle size distribution of small and larger particles.

Reactive deposition of $Ni(Cp)_2$ using H_2 in $scCO_2$ allows to incorporate large quantities of metal. The loadings are similar or larger than those reported by Bozbag et al. (5-6.5% wt.) for other Ni/carbon aerogel materials [31].The mesopore size of the support limits the crystal growth of the particles within the support.

(b) Ni composite materials obtained by impregnation

Experiments were performed on SiO_2 SBA-15 using different precursors: the organometallic $Ni(Cp)_2$ and the inorganic salts $Ni(NO_3)_2{\cdot}6H_2O$ and $NiCl_2{\cdot}6H_2O$. Inorganic metals salts are generally cheaper, less volatile and toxic, and more stable than the organometallic compounds, but they are not soluble in $scCO_2$. However, they can be dissolved in $EtOH/CO_2$ mixtures either in the supercritical or the liquid stated (liquid expanded mixtures) [35].

Impregnation using $Ni(Cp)_2$ was performed at 60 ºC and 11.0 MPa in $scCO_2$. However, impregnation conditions for $Ni(NO_3)_2{\cdot}6H_2O$ and $NiCl_2{\cdot}6H_2O$ salts were changed to 35 ºC and 9.0 MPa, to prevent reduction of the inorganic metal

salts in the EtOH/CO_2 mixture and favour dissolution. After impregnation, samples were reduced in H_2/N_2 at 400ºC in a tubular furnace. In every case, samples turned very dark after reduction, suggesting Ni deposition in the samples.

XRD of the samples obtained by impregnation of $Ni(Cp)_2$ after treatment in H_2/N_2 at 400 ºC did not show clear reflections at ca. 45 º due to Ni, even for the sample with the highest loading (Figure 4). TEM images of the sample impregnated for 3 hours and further reduced in H_2/N_2 are given in Figure 5. At high magnification, very small particles of ca. 2 nm can be made out. Ni content determined from EDX for these samples was ca. 12 Ni mol% (for a maximum loading of ca. 24 mol%). Although $Ni(Cp)_2$ sublimes partially in H_2/N_2, when it is impregnated on the SiO_2 surface, it gets reduced at temperature much lower than 400 ºC (see TGA on supplementary material). Therefore deposition of Ni on the mesopores walls must have been taken place at these conditions. This methodology may to be very effective in producing heterogeneous catalysts.

Further impregnation experiments were performed using $Ni(NO_3)_2{\cdot}6H_2O$ and $NiCl_2{\cdot}6H_2O$ in 9% mol EtOH/CO_2 solutions. Figure 6 shows XRD patterns of the Ni/SiO_2 samples obtained after reduction in H_2/N_2 at 400 ºC. XRD shows intense reflections ascribed to Ni [PDF-040850] in both samples. Peaks are broader for the sample prepared using $Ni(NO_3)_2{\cdot}6H_2O$.

TEM images of the Ni/SiO_2 samples obtained by impregnation using the inorganic salts are shown in Figure 7. Very different results were obtained for the different inorganic precursors. In the sample deposited using $Ni(NO_3)_2{\cdot}6H_2O$, round nanoparticles with a broad particle size distribution were observed on the images. Some of the nanoparticles appeared smaller than the pore size of the support and may have been deposited into the SiO_2 mesopores. Other much larger particles were clearly deposited on the external surface of the support. In the sample deposited using $NiCl_2{\cdot}6H_2O$ however, nanowires ending on large crystals were observed instead of nanoparticles. The very different morphologies obtained with these precursors suggest a different deposition mechanism. Hoang-Van et al. [45] have compared Ni/SiO_2 materials prepared by wet impregnation using nickel chloride and nickel nitrate. The materials prepared using the chloride always exhibited low metal dispersion. This has been related to the high volatility of nickel chloride in the presence of hydrogen and hydrogen chloride (reduction by-product), which may yield large crystals (in this case nanowires) whereas the small ones tend to vaporize and disappear completely. The phase behaviour of the different salts in the EtOH/CO_2 solution may also play a role. Further experiments studying the metal deposition mechanism for the different salts would be required.

(c) Ni composite materials obtained by reactive deposition using ethanol

Experiments were performed on SiO_2 SBA-15 and the carbon xerogel C14 using different organometallic precursors: $Ni(cp)_2$, $Ni(hfac)_2{\cdot}2H_2O$ and $Ni(acac)_2$.

$Ni(hfac)_2{\cdot}2H_2O$ is not very soluble in $scCO_2$ (mole fraction y = $8.3\ 10^{-5}$ at 60 ºC and 15.1 MPa), but its solubility can be increased almost two orders of magnitude by a adding a small amount of ethanol 2-6.5% mol EtOH/CO_2 [46]. Similarly, $Ni(acac)_2$ is scarcely soluble in pure CO_2 (mole fraction y = $6.0\ 10^{-5}$ at 60 ºC and 30.0 MPa) [28]. For this precursor, a similar solubility increase to that observed for $Ni(hfac)_2{\cdot}2H_2O$ in EtOH/CO_2 may be expected.

Experiments performed using $Ni(hfac)_2{\cdot}2H_2O$ and $Ni(acac)_2$ on SiO_2 SBA-15 and C14 were carried out loading the precursor, the substrate and a small amount of ethanol into the reactor and adding CO_2 at 80 ºC and 13.5 MPa (9-20% mol EtOH/CO_2). Conditions were chosen to promote metal adsorption on the support, by assuring sufficient solubilization of the precursor. Then the reactor was heated at 150-200 ºC to start the metal reduction by the alcohol. In these examples, EtOH acted both as cosolvent and reducing agent.

Experiments performed using $Ni(hfac)_2{\cdot}2H_2O$ on SiO_2 SBA-15 were unsuccessful and after depressurization the white SiO_2 support was recovered from the reactor. Ethanol adsorbs strongly on the hydrophilic SiO_2 surface and may hinder adsorption of the metal precursor on the SiO_2 support.

Deposition however proceeded readily on the carbon xerogel from 150 ºC. Figure 8 shows XRD patterns of the Ni/C14 samples deposited using $Ni(hfac)_2{\cdot}2H_2O$ and $Ni(acac)_2$ at 200ºC in 10% mol EtOH/CO_2. In both cases, very broad bands at 44.5 º ascribed to Ni are observed. An average particle size of 2 nm was estimated using the Sherrer equation.

TEM images of the sample obtained using $Ni(hfac)_2{\cdot}2H_2O$ following this procedure are shown in Figure 9. Due to the very small particle size, it is very difficult to visualize the Ni nanoparticles. In comparison to the materials obtained by reactive deposition using H_2, the metal nanoparticles in this case are much smaller. EtOH is a weak reductant in comparison to H_2 and at the same temperature tend to give smaller particles.

In these experiments, during depressurization, the reaction mixture was bubbled through acetone. In every case, the acetone solutions recovered were coloured, suggesting incomplete decomposition of the precursor. Furthermore, in some experiments, the colour of the solution changed from green (colour of the precursor in acetone) to red. This has been related to the possible reaction of $Ni(hfac)_2{\cdot}2H_2O$ with EtOH [46]. The formation of ethanol adducts with nickel acetylacetonate [$Ni(acac)_2{\cdot}2EtOH$] has been also previously reported [47, 48]. This side reaction was observed at the highest temperature and may hinder the deposition process.

Finally, $Ni(Cp)_2$ was also used in the reactive deposition with EtOH on SiO_2. In this experiment, the reactor containing the precursor and a given amount of $Ni(Cp)_2$ was filled with pure CO_2 at 60 ºC and 9.0 MPa. Because of the much higher solubility of this precursor, ethanol was introduced just after the impregnation step using a high-pressure HPLC six-way valve, flowing CO_2 at constant temperature up to 11.0 MPa (4% mol EtOH/CO_2). The reactor was then heated to 200 ºC to promote the metal reduction. Figure 10 shows XRD pattern of the Ni/SiO_2 composite material. A very

weak peak at 44.5º was ascribed to the presence of Ni. Although Ni nanoparticles could not be observed on the TEM images, EDX analysis of this sample showed Ni percentages between 4-10% mol. In some regions, a high carbon content was also measured, suggesting incomplete decomposition of this precursor and these conditions. This sample was heat-treated in air at 400 ºC for 5 hours. XRD of the calcined sample is also shown in Figure 10. XRD pattern showed the presence of NiO [PDF-780643]. New peaks are weak and broad, but more intense than those obtained before calcination, which suggests the partial reduction of $Ni(Cp)_2$ in $EtOH/CO_2$ at 200 ºC. Figure 11 shows TEM images of the sample obtained by ethanol reduction using $Ni(Cp)_2$ at 200 ºC after calcination in air at 400 ºC. Very small nanoparticles of 1-2 nm can be observed in the TEM. The complete decomposition of $Ni(Cp)_2$ on SiO_2 in the CO_2/EtOH mixture seems to require temperatures higher than 200 ºC.

4. Conclusions

Ni nanoparticles were successfully deposited into mesoporous SiO_2 SBA-15 and a carbon xerogel using $scCO_2$. Different Ni precursors and methodologies were used. The good transport properties of $scCO_2$ allowed introducing metal precursors into the pores of the support without damaging its structure.

Reactive deposition using H_2 in $scCO_2$ at 200-250 ºC yielded Ni nanoparticles within the mesopores of the support. With this method, the size of the nanoparticles was limited in each case by the pore size of the support (below 6 and 14 nm for mesoporous SiO_2 SBA-15 and the mesoporous carbon C14, respectively). However, larger particles were also observed on the external surface of the supports. Large metal loadings were incorporated into the material using his method.

In contrast, smaller Ni nanoparticles of ca. 2 nm observed by TEM were deposited on SiO_2 SBA-15 by impregnation of $Ni(Cp)_2$ in $scCO_2$ and reduction in H_2/N_2 at 400 ºC at low pressure. This is the method that gives normally the smallest metal nanoparticles. Nevertheless, the amount of metal that can be loaded is limited by the adsorption equilibrium and, for some precursors, if the adsorption of the precursor on the support is weak, partial sublimation of the precursor during the thermal treatment may be produced.

Impregnation with $Ni(NO_3)_2{\cdot}6H_2O$ and $NiCl_2{\cdot}6H_2O$ in $EtOH/CO_2$ and reduction in H_2/N_2 at 400 ºC at low pressure was also attempted. These precursors are less toxic, cheaper and easier to handle than the nickel organometallic compounds, therefore the interest of exploring its use in metal deposition from supercritical fluids. Impregnation using $Ni(NO_3)_2{\cdot}6H_2O$ yielded larger round nanoparticles on the support, whilst impregnation using $NiCl_2{\cdot}6H_2O$ yielded nanowires. The different morphologies could be related to the different decomposition mechanism of these salts. Further studies should be conducted using $Ni(NO_3)_2{\cdot}6H_2O$ to try to optimize reaction conditions and favour deposition of smaller nickel nanoparticles. The formation of nickel nanowires into the SiO_2 supports using $NiCl_2{\cdot}6H_2O$ should be also explored for its application in magnetic and electronic devices.

Finally, the reactive deposition of $Ni(hfac)_2{\cdot}2H_2O$, and $Ni(acac)_2$ using ethanol in $scCO_2$ at 150-200 ºC was only successful on the cabon xerogel, probably due to its reducing character, yielding the smallest Ni nanoparticle. The possible reaction of EtOH with these precursor forming adducts at high temperature and long times may limit its application.

Supercritical CO_2 is a green solvent that allows the deposition of metal nanoparticles into high surface area mesoporous supports. In the material obtained by impregnation of $Ni(Cp)_2$ on SiO_2 and reduction in H_2/N_2 at 400ºC and those obtained by reactive deposition of $Ni(hfac)_2{\cdot}2H_2O$ and $Ni(acac)_2$ on carbon using $EtOH/CO_2$, Ni nanoparticles on the support were very small and were very homogeneously distributed within the support. These are the structural properties desired in a heterogeneous catalyst. Catalytic test of these materials should be conducted.

Additional Information

Acknowledgments

We thank Prof. M.J. Torralvo for assistance with the N_2-Adsorption experiments and Prof. J.A.R. Renuncio for helpful discussion. We acknowledge "ICTS- Centro Nacional de Microscopía Electrónica" and "Centro de Rayos X" at UCM for technical assistance.
A. Cabañas would like to acknowledge Prof. Sir Martyn Poliakoff for introducing her into the fields of Green Chemistry and Materials Science.

Funding Statement

We gratefully acknowledge the financial support of the Spanish Ministry of Economy and Competitiveness (MINECO), research projects CTQ2013-41781 and MAT2012-39199-C02-02.
J. Morere thanks MINECO for his support through a predoctoral grant. P. Palomino thanks UCM for his support through a predoctoral grant

Competing Interests

We have no competing interests.

Authors' Contributions

Albertina Cabañas designed the experiments, interpreted the results and wrote the manuscript.
The PhD student Jacobo Morere supervised the nickel deposition experiments carried out by the undergraduate students Sergio Royuela and Guillermo Asensio, synthesized the SiO_2 SBA-15 support and performed the materials characterization.

Pablo Palomino and Eduardo Enciso synthesized the carbon xerogel support and characterized it.
Concepción Pando contributed to the analysis and interpretation of the data and critically revised the manuscript.

References

[1] Blackburn, J.M., Long, D.P., Cabanas, A. & Watkins, J.J. 2001 Deposition of conformal copper and nickel films from supercritical carbon dioxide. *Science* **294**, 141-145. (doi:10.1126/science.1064148).

[2] Hunde, E.T. & Watkins, J.J. 2004 Reactive deposition of cobalt and nickel films from their metallocenes in supercritical carbon dioxide solution. *Chem. Mater.* **16**, 498-503. (doi:10.1021/cm034433n).

[3] Polshettiwar, V., Baruwati, B. & Varma, R.S. 2009 Nanoparticle-supported and magnetically recoverable nickel catalyst: a robust and economic hydrogenation and transfer hydrogenation protocol. *Green Chemistry* **11**, 127-131. (doi:10.1039/B815058C).

[4] Azadi, P., Farnood, R. & Meier, E. 2010 Preparation of Multiwalled Carbon Nanotube-Supported Nickel Catalysts Using Incipient Wetness. *Method. J Phys Chem A.* **114**, 3962-3968. (doi:10.1021/jp907403b).

[5] De Jesus, J., Gonzalez, I., Garcia, M. & Urbina, C. 2008 Preparation of nickel nanoparticles and their catalytic activity in the cracking of methane. *J. Vac. Sci. Technol. A.* **26**, 913-918. (doi:10.1116/1.2885212).

[6] Kukovitsky, E.F., L'Vov, S.G. & Sainov, N.A. 2000 VLS-growth of carbon nanotubes from the vapor *Chem. Phys. Lett.* **317**, 65-70 (doi:10.1016/S0009-2614(99)01299-3).

[7] Singh, B., Laffir, F., Dickinson, C., McCormac, T. & Dempsey, E. 2011 Carbon Supported Cobalt and Nickel Based Nanomaterials for Direct Uric Acid Determination. . *Electroanalysis* **23**, 79-89. (doi:10.1002/elan.201000444).

[8] Schmid, G. 2008 General Features of Metal Nanoparticles Physics and Chemistry In *Metal Nanoclusters in Catalysis and Materials Science. The Issue of Size Control* (ed. B. Corain, G. Schmid and N. Toshima), Elsevier B.V.,Amsterdam.

[9] Kamat, P.V. 2002 Photophysical, photochemical and photocatalytic aspects of metal nanoparticles. *J. Phys. Chem. B* **106**, 7729-7744. (doi:10.1021/jp0209289).

[10] Rao, C.N.R., Kulkarni, G.U., Thomas, P.J. & Edwards, P.P. 2000 Metal nanoparticles and their assemblies. *Chem. Soc. Rev.* **29**, 27-35. (doi:10.1039/a904518j).

[11] Astruc, D., Lu, F. & Aranzaes, J.R. 2005 Nanoparticles as recyclable catalysts: The frontier between homogeneous and heterogeneous catalysis. *Angew. Chem. Inter. Ed.* **44**, 7852-7872. (doi:10.1002/anie.200500766).

[12] White, R.J., Luque, R., Budarin, V.L., Clark, J.H. & Macquarrie, D.J. 2009 Supported metal nanoparticles on porous materials. Methods and applications. *Chem. Soc. Rev.* **38**, 481-494. (doi:10.1039/b802654h).

[13] Saha, K., Agasti, S.S., Kim, C., Li, X. & Rotello, V.M. 2012 Gold Nanoparticles in Chemical and Biological Sensing. *Chem. Rev.* **112**, 2739-2779. (doi:10.1021/cr2001178).

[14] Burda, C., Chen, X.B., Narayanan, R. & El-Sayed, M.A. 2005 Chemistry and properties of nanocrystals of different shapes. *Chem. Rev.* **105**, 1025-1102. (doi:10.1021/cr030063a).

[15] Beckman, E.J. 2004 Supercritical and near-critical CO2 in green chemical synthesis and processing. *J. Supercrit. Fluids* **28**, 121–191. (doi:10.1016/S0896-8446(03)00029-9).

[16] Poling, B.E., Prausnitz, J.M. & O´Connell, J.P. 2001 *The Properties of Gases and Liquids*. International Edition ed. Singapore, McGraw-Hill

[17] Bourne, R.A. & Poliakoff, M. 2011 Green chemistry: what is the way forward? *Mendeleev. Commun.* **21**, 235-238. (doi:10.1016/j.mencom.2011.09.001).

[18] Stevens, J.G., Gomez, P., Bourne, R.A., Drage, T.C., George, M.W. & Poliakoff, M. 2011 Could the energy cost of using supercritical fluids be mitigated by using CO2 from carbon capture and storage (CCS)? *Green Chemistry* **13**, 2727-2733. (doi:10.1039/C1GC15503B).

[19] Darr, J.A. & Poliakoff, M. 1999 New Directions in Inorganic and Metal-Organic Coordination Chemistry in Supercritical Fluids. *Chem. Rev.* **99**, 495-541. (doi:10.1021/cr970036i).

[20] Morley, K.S., Licence, P., Marr, P.C., Hyde, J.R., Brown, P.D., Mokaya, R., Xia, Y.D. & Howdle, S.M. 2004 Supercritical fluids: A route to palladium-aerogel nanocomposites. *J. Mater. Chem.* **14**, 1212-1217. (doi:10.1039/b311065f).

[21] Sánchez-Vicente, Y., L., S., Pando, C., Torralvo, M.J., Snape, C.E., Drage, T.C. & Cabañas, A. 2015 A new sustainable route in supercritical CO2 to functionalize silica SBA-15 with 3-aminopropyltrimethoxysilane as material for carbon capture. *Chem. Eng. J.* **264** 886–898. (doi:10.1016/j.cej.2014.12.002).

[22] Sanchez-Vicente, Y., Pando, C., Cortijo, M. & Cabanas, A. 2014 Chemical surface modification of mesoporous silica SBA-15 with a tertiary aminosilane using supercritical carbon dioxide. *Micropor. Mesopor. Mater.* **193**, 145-153. (doi:10.1016/j.micromeso.2014.03.021).

[23] Erkey, C. 2009 Preparation of metallic supported nanoparticles and films using supercritical fluid deposition. *J. Supercrit. Fluids* **47**, 517-522. (doi:10.1016/j.supflu.2008.10.019).

[24] Zhang, Y. & Erkey, C. 2006 Preparation of supported metallic nanoparticles using supercritical fluids: A review. *J. Supercrit. Fluids* **38**, 252-267. (doi:10.1016/j.supflu.2006.03.021).

[25] Tenorio, M.J., Pando, C., Renuncio, J.A.R., Stevens, J.G., Bourne, R.A., Poliakoff, M. & Cabanas, A. 2012 Adsorption of Pd(hfac)2 on mesoporous silica SBA-15 using supercritical CO2 and its role in the performance of Pd-SiO2 catalyst. *J. Supercrit. Fluids* **69**, 21-28. (doi:10.1016/j.supflu.2012.05.003).

[26] Morere, J., Tenorio, M.J., Torralvo, M.J., Pando, C., Renuncio, J.A.R. & Cabanas, A. 2011 Deposition of Pd into mesoporous silica SBA-15 using supercritical carbon dioxide. *J. Supercrit. Fluids* **56**, 213-222. (doi:10.1016/j.supflu.2010.12.012).

[27] Morere, J., Torralvo, M.J., Pando, C., Renuncio, J.A.R. & Cabanas, A. 2015 Supercritical fluid deposition of Ru nanoparticles into SiO2 SBA-15 as a sustainable method to prepare selective hydrogenation catalysts. *RSC Advances* **5**, 38880 - 38891 (doi:10.1039/C5RA04969E).

[28] Aschenbrenner, O., Kemper, S., Dahmen, N., Schaber, K. & Dinjus, E. 2007 Solubility of beta-diketonates, cyclopentadienyls, and cyclooctadiene complexes with various metals in supercritical carbon dioxide. *J. Supercrit. Fluids* **41**, 179-186. (doi:10.1016/j.supflu.2006.10.011).

[29] Romang, A.H. & Watkins, J.J. 2010 Supercritical Fluids for the Fabrication of Semiconductor Devices: Emerging or Missed Opportunities? *Chem. Rev.* **110**, 459-478. (doi:10.1021/cr900255w).

[30] Peng, Q., Spagnola, J.C. & G.N., P. 2008 Self-catalyzed hydrogenolysis of nickelocene: Functional metal coating of three-dimensional nanosystems at low temperature. *J. Electrochem. Soc.* **155**, D580-D582. (doi:10.1149/1.2946723).

[31] Bozbag, S.E., Zhang, L.C., Aindow, M. & Erkey, C. 2012 Carbon aerogel supported nickel nanoparticles and nanorods using supercritical deposition. *J. Supercrit. Fluids* **66**, 265-273. (doi:10.1016/j.supflu.2012.02.027).

[32] Liu, Z.M. & Sun, Z.Y. 2010 Green solvent-based approaches for synthesis of nanomaterials. *Sci. China-Chem.* **53**, 372-382. (doi:10.1007/s11426-010-0040-0).

[33] Sun, Z., Zhang, X., Han, B., Wu, Y., An, G., Liu, Z., Miao, S. & Miao, Z. 2007 Coating carbon nanotubes with metal oxides in a supercritical carbon dioxide-ethanol solution. *Carbon* **45**, 2589-2596. (doi:10.1016/j.carbon.2007.08.016).

[34] Sun, Z.Y., Fu, L., Liu, Z.M., Han, B.X., Liu, Y.Q. & Du, J.M. 2006 Synthesis of noble metal/carbon nanotube composites in supercritical methanol. *J. Nanosci. Nanotechnol.* **6**, 691-697. (doi:10.1166/jnn.2006.128).

[35] Ming, J., Wu, C., Cheng, H., Yu, Y. & Zhao, F. 2011 Reaction of hydrous inorganic metal salts in CO2 expanded ethanol: Fabrication of nanostructured materials via supercritical technology. *J. Supercrit. Fluids* **57**, 137-142. (doi:10.1016/j.supflu.2011.03.003).
[36] Zhao, D.Y., Huo, Q.S., Feng, J.L., Chmelka, B.F. & Stucky, G.D. 1998 Nonionic triblock and star diblock copolymer and oligomeric surfactant syntheses of highly ordered, hydrothermally stable, mesoporous silica structures. *J. Am. Chem. Soc.* **120**, 6024-6036. (doi:10.1021/ja974025i).
[37] Zhao, D.Y., Feng, J.L., Huo, Q.S., Melosh, N., Fredrickson, G.H., Chmelka, B.F. & Stucky, G.D. 1998 Triblock copolymer syntheses of mesoporous silica with periodic 50 to 300 angstrom pores. *Science* **279**, 548-552. (doi:10.1126/science.279.5350.548).
[38] Al-Muhtaseb, S. & Ritther, J.A. 2003 Preparation and Properties of Resorcinol-Formaldehyde Organic and Carbon Gels. *Adv. Mater.* **15**, 101-114. (doi:10.1002/adma.200390020).
[39] Barroso-Bujans, F., Palomino, P., Cerveny, S., Fernandez-Alonso, F., Rudic, S., Alegria, A., Colmenero, J. & Enciso, E. 2013 Confinement of poly(ethylene oxide) in the nanometer-scale pores of resins and carbon nanoparticles. *Soft Matter* **9**, 10960-10965. (doi:10.1039/c3sm51563j).
[40] Olivares-Marin, M., Palomino, P., Enciso, E. & Tonti, D. 2014 Simple Method to Relate Experimental Pore Size Distribution and Discharge Capacity in Cathodes for Li/O-2 Batteries. *J. Phys. Chem. C* **118**, 20772-20783. (doi:10.1021/jp5053453).
[41] Jaroniec, M., Kruk, M. & Olivier, J.P. 1999 Standard Nitrogen Adsorption Data for Characterization of Nanoporous Silicas. *Langmuir* **15**, 5410-5413. (doi:10.1021/la990136e).
[42] Barret, E., Joyner, L.G. & Halenda, P.P. 1951 The determination of pore volume and area distributions in porous substances. I. Computations for nitrogen isotherms. *J. Am. Chem. Soc.* **73**, 373-380. (doi:10.1021/ja01145a126).
[43] Kurk, M., Janoriec, M., ko, C.H. & Ryoo, R. 2000 Characterization of the porous structure of SBA-15. *Chem. Mater.* **12**, 1961-1968. (doi:10.1021/cm000164e).
[44] Meynen, V., Cool, P. & Vansant, E.F. 2007 Synthesis of siliceous materials with micro- and mesoporosity. *Micropor. Mesopor. Mater.* **104**, 26-38. (doi:10.1016/j.micromeso.2006.12.003).
[45] Hoangvan, C., Kachaya, Y., Teichner, S.J., Arnaud, Y. & Dalmon, J.A. 1989 Characterization of Nickel-catalysts by chemisorption techniques, X-ray diffraction and magnetic measurements- Effects of support, precurosr and hydrogen pretreatment. *Appl. Catal.* **46**, 281-296. (doi:10.1016/s0166-9834(00)81123-9).
[46] Tenorio, M.J., Cabañas, A., Pando, C. & Renuncio, J.A.R. 2010 Solubility of Pd(hfac)2 and Ni(hfac)2·2H2O in supercritical carbon dioxide pure and modified with ethanol. *J. Supercrit. Fluids* **70**, 106-111. (doi:10.1007/BF01236639).
[47] Pfluger, C.E., Burke, T.S. & Bednowitz, A.L. 1973 Crystal and molecular structure of bis(acetylacetonato) nickel(II)diethanol. *J. Crystal and Molecular Structure* **3**, 181-191. (doi:10.1007/BF01236639).
[48] Polyakov, V.R. & Czerwinski, M. 2001 Hydrogen-bonding in ethanol adducts to bis(3-R-penta-2,4-dionato)nickel(II) species. *Inorg. Chem.* **40**, 4798-4802. (doi:10.1021/ic991284v).

Tables

Table 1. Summary of the deposition experiments showing for the different methodologies, precursors and supports: the impregnation and reduction conditions, the EtOH mol percentage in CO_2, the maximum Ni loading considering the initial precursor and support quantities and the actual Ni mol percentage measured by EDX analysis on the Ni/SiO_2 SBA-15 samples. The particle size and morphology based on the TEM images is also given.

Methodology	Support	Precursor	impregnation		Reduction	%EtOH mol	max. Ni loading		EDX (% mol)	Particle size/ Morphology
			T/ºC	P/MPa	T/ºC		% mol	% wt.		
Reactive deposition H_2	SBA-15	$Ni(Cp)_2$	60	11.0	200	-	9.1	8.9	up to 13%	small (< 6 nm) and larger (20-30 nm)
			60	9.5	250	-	14.9	14.6	4.3	small (< 6 nm) and larger (20-30 nm)
	C14	$Ni(Cp)_2$	60	11.0	200	-	2.4	10.6	-	10-25 nm (14-15 nm by Scherrer)
Impregnation	SBA-15	$Ni(Cp)_2$	60	11.0	400[a]	-	8.8	8.6	-	< 2 nm
			60	11.0	400[a]	-	24.0	23.6	up to 12%	< 2 nm
		$Ni(NO_3)_2{\cdot}6H_2O$	35	9.0	400[a]	9%	67.6	67.1	50%	large round crystals
		$NiCl_2{\cdot}6H_2O$	35	9.0	400[a]	9%	71.5	71.0	-	Nanowires and large crystals
Reactive deposition EtOH	SBA-15	$Ni(hfac)_2.2H_2O$	80	13.5	150	10%	5.4	5.3	-	-
			80	13.5	200	15%	5.8	5.6	-	-
			80	13.5	150	20%	5.7	5.6	-	-
		$Ni(Cp)_2$	60	11.0	200	4%	14.3	14.0	4-10%	1-2 nm
	C14	$Ni(hfac)_2.2H_2O$	80	13.5	200	10%	1.3	6.0	-	2 nm
			80	13.5	150	15%	1.3	5.9	-	2 nm
			80	13.5	200	20%	1.2	5.8	-	2 nm
		$Ni(acac)_2$	80	13.5	200	10%	2.2	10.1	-	2 nm
			80	13.5	150	15%	2.3	10.2	-	2 nm
			80	13.5	200	20%	2.2	10.0	-	2 nm

[a]Reduction in 5% mol H_2/N_2 at atmospheric pressure in a tubular furnace

Figure and table captions

Table 1. Summary of the deposition experiments showing for the different methodologies, precursors and supports: the impregnation and reduction conditions, the EtOH mol percentage in CO_2, the maximum Ni loading considering the initial precursor and support quantities and the actual Ni mol percentage measured by EDX analysis on the Ni/SiO_2 SBA-15 samples. The particle size and morphology based on the TEM images is also given.

Figure 1. XRD patterns for samples prepared by H_2 reduction of $Ni(Cp)_2$ in $scCO_2$ at 200 ºC: (a) Ni/SiO_2 SBA-15, (b) Ni/C14 and (c) Ni/SiO_2 SBA-15 heated in air at 400 ºC.

Figure 2. TEM images of Ni/SiO_2 SBA-15 samples prepared by H_2 reduction of $Ni(Cp)_2$ in $scCO_2$ at: (a,b) 200 ºC, (c,d) 250 ºC and (e,f) 200 ºC followed by calcination in air at 400 ºC.

Figure 3. TEM images of a Ni/C14 samples prepared by H_2 reduction of $Ni(Cp)_2$ in $scCO_2$ at 200 ºC.

Figure 4. XRD pattern of a Ni/SiO_2 SBA-15 sample obtained by impregnation of $Ni(Cp)_2$ in $scCO_2$ and further reduction in H_2/N_2 at 400ºC.

Figure 5. TEM images of a Ni/SiO_2 SBA-15 sample obtained by impregnation of $Ni(Cp)_2$ in $scCO_2$ and further reduction in H_2/N_2 at 400ºC.

Figure 6. XRD patterns of the Ni/SiO_2 SBA-15 samples prepared by impregnation in $scCO_2$ and further reduction in H_2/N_2 at 400 ºC using: (a) $Ni(NO_3)_2{\cdot}6H_2O$ and (b) $NiCl_2{\cdot}6H_2O$.

Figure 7. TEM images of the Ni/SiO_2 SBA-15 samples prepared by impregnation in $scCO_2$ and further reduction in H_2/N_2 at 400 ºC using: (a,b) $Ni(NO_3)_2{\cdot}6H_2O$ and (c,d) $NiCl_2{\cdot}6H_2O$.

Figure 8. XRD patterns of Ni/C14 samples prepared by ethanol reduction at 200 ºC in 10 % $EtOH/CO_2$ using (a) $Ni(hfac)_2{\cdot}2H_2O$ and (b) $Ni(acac)_2$.

Figure 9. TEM images of a Ni/C14 sample prepared by ethanol reduction of $Ni(hfac)_2{\cdot}2H_2O$ /CO_2 at 200 ºC in 10 % $EtOH/CO_2$.

Figure 10. XRD patterns of Ni/SiO_2 SBA-15 samples prepared by ethanol reduction of $Ni(Cp)_2$ at 200 ºC in 10 % $EtOH/CO_2$: (a) as deposited and (b) after calcination at 400 ºC.

Figure 11. TEM images of a Ni/SiO_2 SBA-15 sample prepared by ethanol reduction of $Ni(Cp)_2$ at 200 ºC in 10 % $EtOH/CO_2$ after calcination at 400 ºC.

Supplementary material

TGA of $Ni(Cp)_2$ and a Ni/SiO_2 SBA-15 sample impregnated with $Ni(Cp)_2$ in $scCO_2$ before reduction are given as supplementary material.

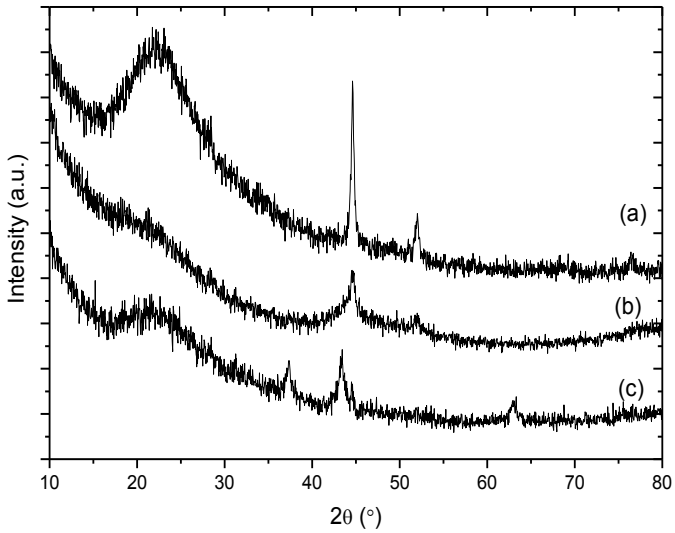

Figure 1. XRD patterns for samples prepared by H_2 reduction of $Ni(Cp)_2$ in $scCO_2$ at 200 ºC: (a) Ni/SiO_2 SBA-15, (b) Ni/C14 and (c) Ni/SiO_2 SBA-15 heated in air at 400 ºC.

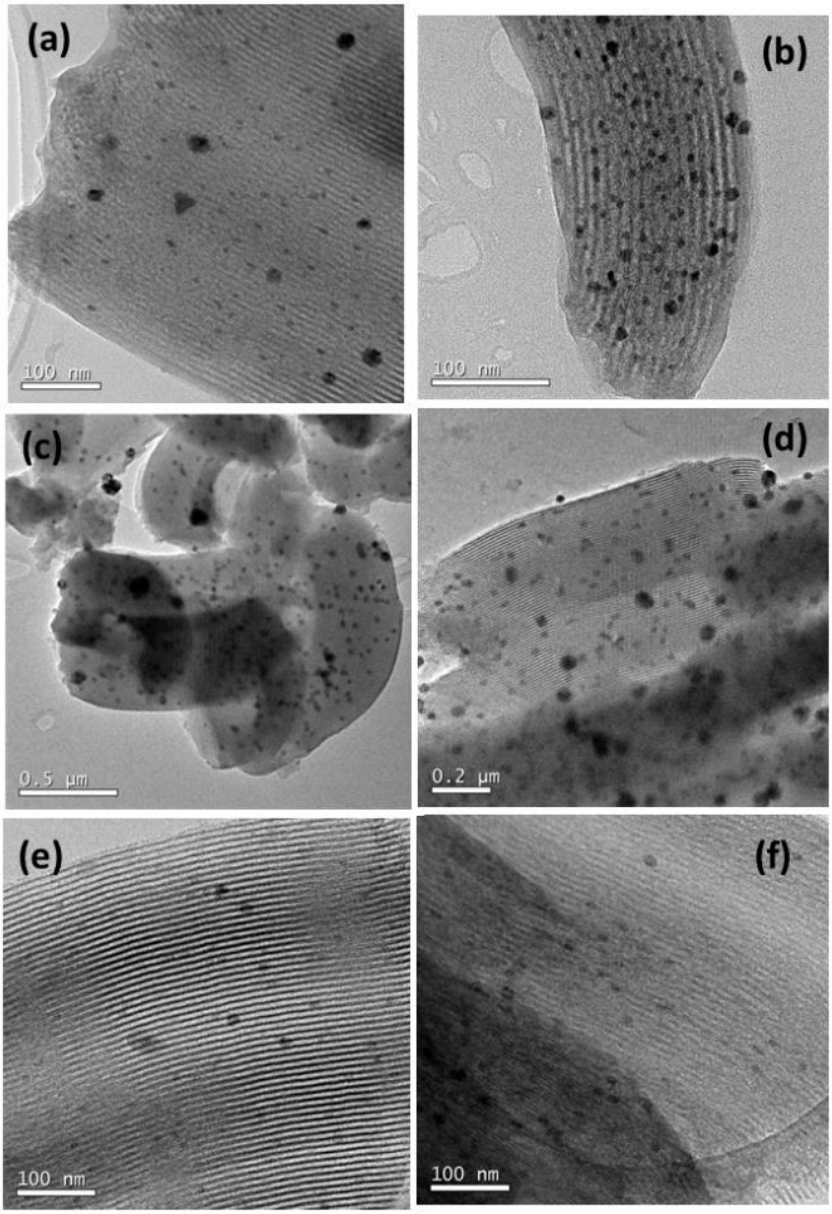

Figure 2. TEM images of Ni/SiO_2 SBA-15 samples prepared by H_2 reduction of $Ni(Cp)_2$ in $scCO_2$ at: (a,b) 200 ºC, (c,d) 250 ºC and (e,f) 200 ºC followed by calcination in air at 400 ºC.

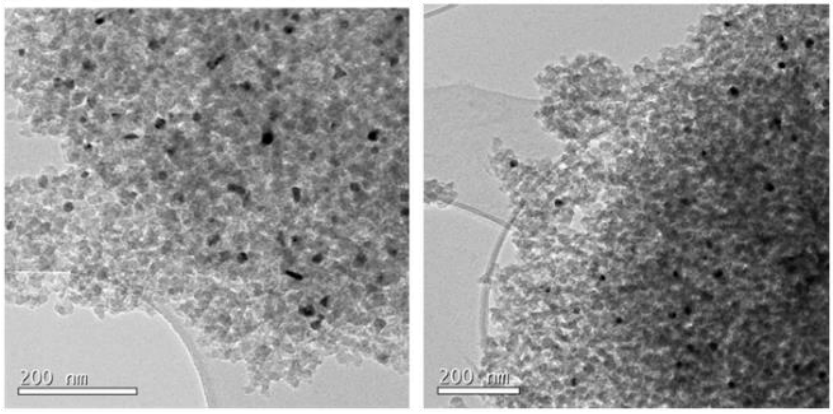

Figure 3. TEM images of Ni/C14 samples prepared by H_2 reduction of $Ni(Cp)_2$ in $scCO_2$ at 200 ºC.

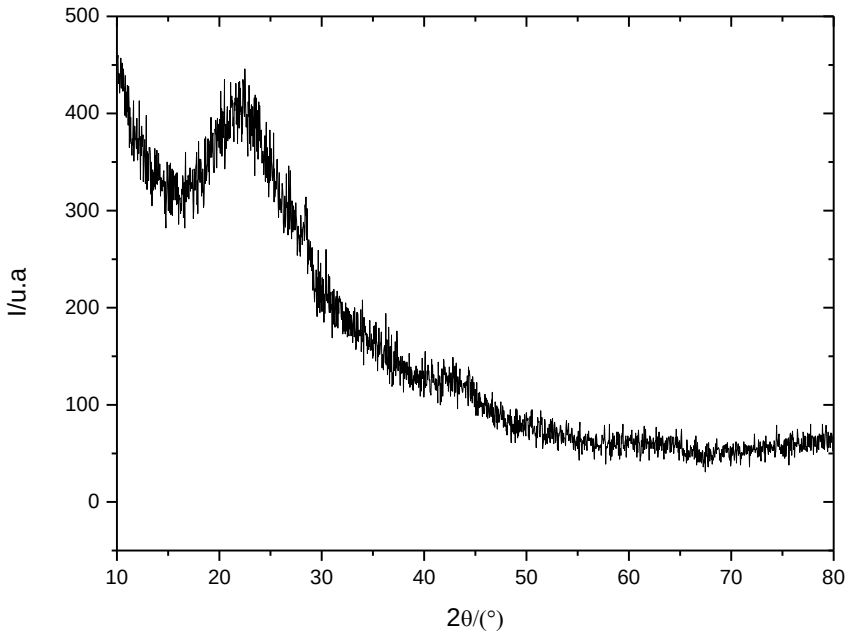

Figure 4. XRD pattern of a Ni/SiO_2 SBA-15 sample obtained by impregnation of $Ni(Cp)_2$ in $scCO_2$ and further reduction in H_2/N_2 at 400ºC.

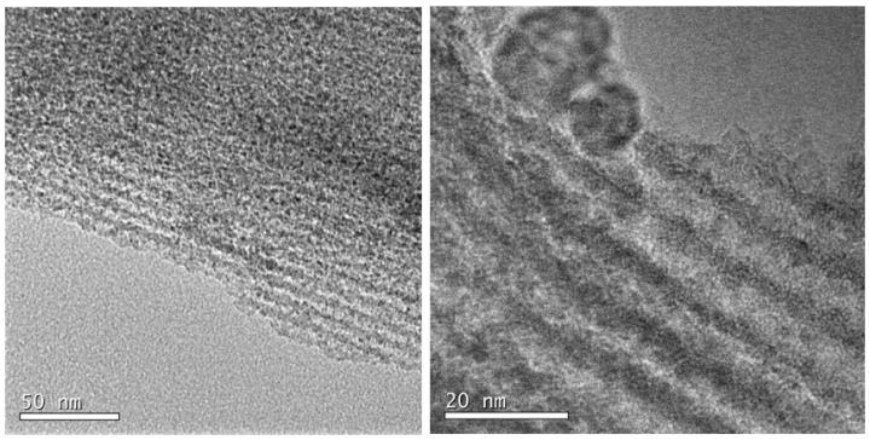

Figure 5. TEM images of a Ni/SiO_2 sample obtained by impregnation of $Ni(Cp)_2$ in $scCO_2$ and further reduction in H_2/N_2 at 400ºC.

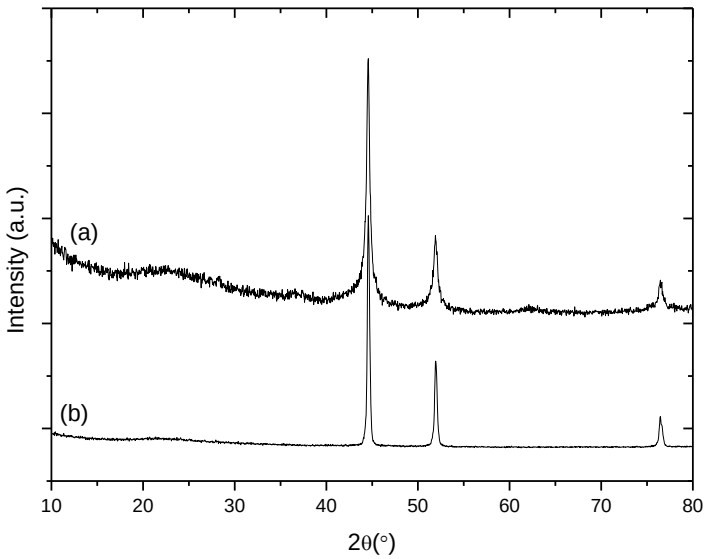

Figure 6. XRD pattern of the Ni/SiO_2 SBA-15 samples prepared by impregnation in $scCO_2$ and further reduction in H_2/N_2 at 400 ºC using: (a) $Ni(NO_3)_2 \cdot 6H_2O$ and (b) $NiCl_2 \cdot 6H_2O$.

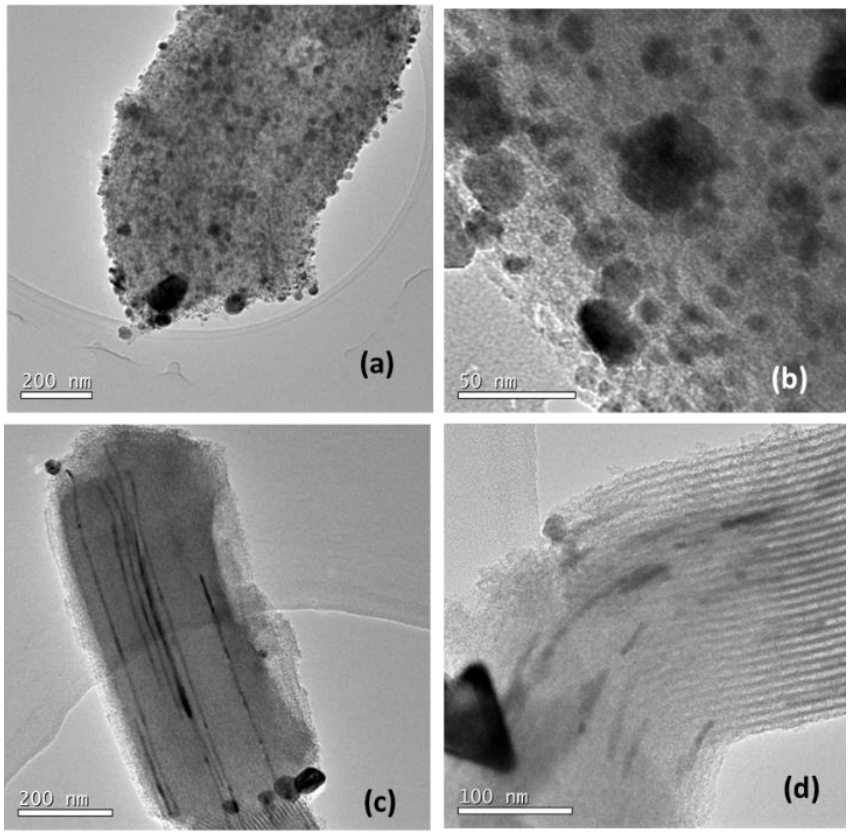

Figure 7. TEM images of the Ni/SiO_2 SBA-15 samples prepared by impregnation in scCO_2 and further reduction in H_2/N_2 at 400 ºC using: (a,b) $Ni(NO_3)_2 \cdot 6H_2O$ and (c,d) $NiCl_2 \cdot 6H_2O$.

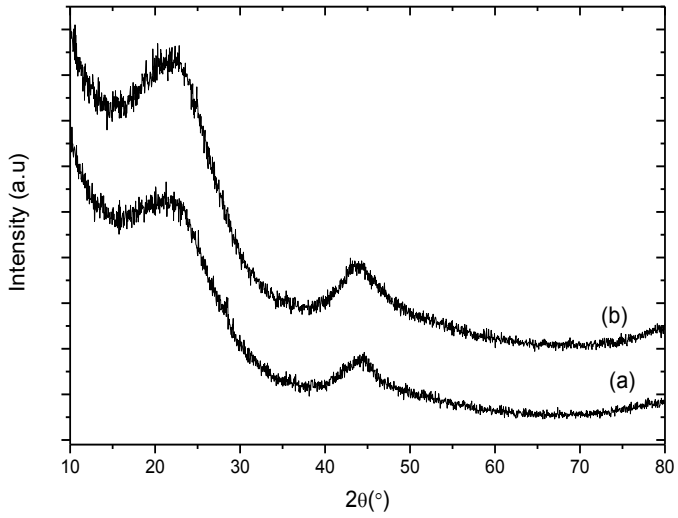

Figure 8. XRD patterns of Ni/C14 samples prepared by ethanol reduction at 200 ºC in 10 % EtOH/CO_2 using (a) Ni(hfac)$_2$·2H_2O and (b) Ni(acac)$_2$

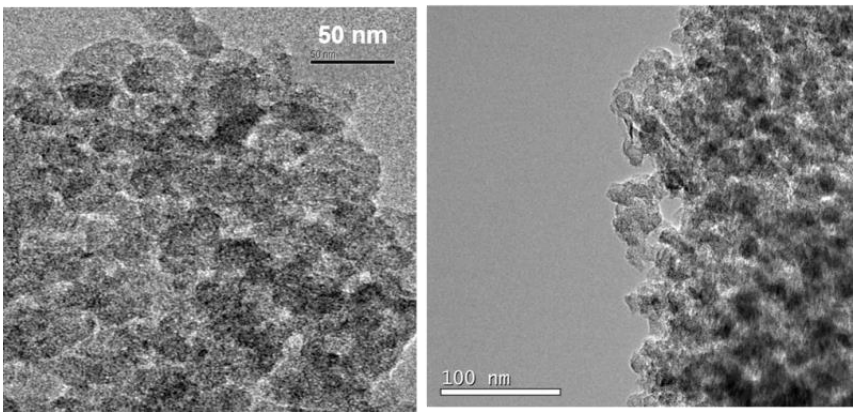

Figure 9. TEM images of a Ni/C14 sample prepared by ethanol reduction of $Ni(hfac)_2 \cdot 2H_2O$ /CO_2 at 200 ºC in 10 % EtOH/CO_2.

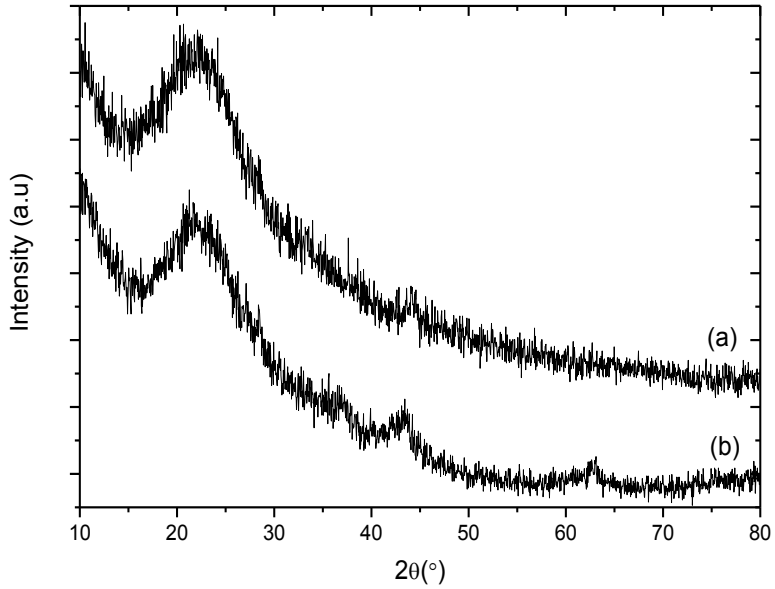

Figure 10. XRD patterns of Ni/SiO_2 SBA-15 samples prepared by ethanol reduction of $Ni(Cp)_2$ at 200 ºC in 10 % $EtOH/CO_2$: (a) as deposited and (b) after calcination at 400 ºC.

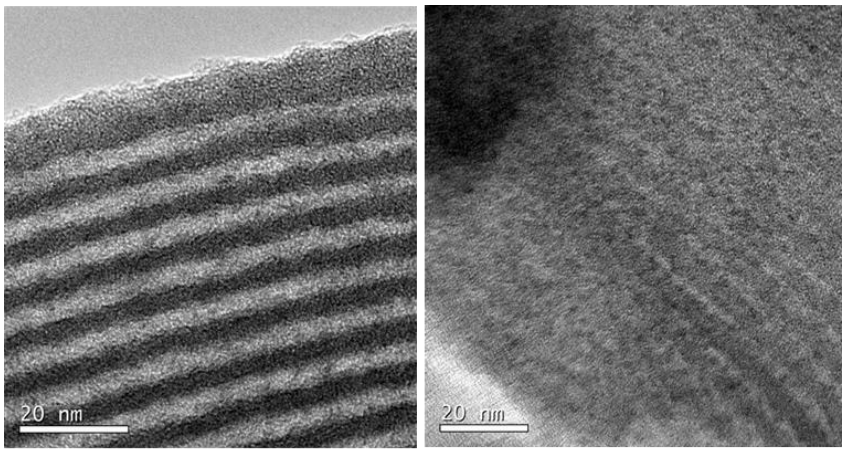

Figure 11. TEM images of a Ni/SiO_2 SBA-15 sample prepared by ethanol reduction of $Ni(Cp)_2$ at 200 ºC in 10 % $EtOH/CO_2$ after calcination at 400 ºC.

Deposition of Ni nanoparticles onto porous supports using supercritical CO_2: effect of the precursor and reduction methodology

Jacobo Morère, Sergio Royuela, Guillermo Asensio, Pablo Palomino, Eduardo Enciso, Concepción Pando and Albertina Cabañas*

Department of Physical-Chemistry I, Universidad Complutense, Ciudad Universitaria s/n, 28040 Madrid, Spain

Keywords: Metal deposition, Nickel nanoparticles, Supercritical CO_2, Mesoporous SiO_2 SBA-15, Mesoporous Carbon

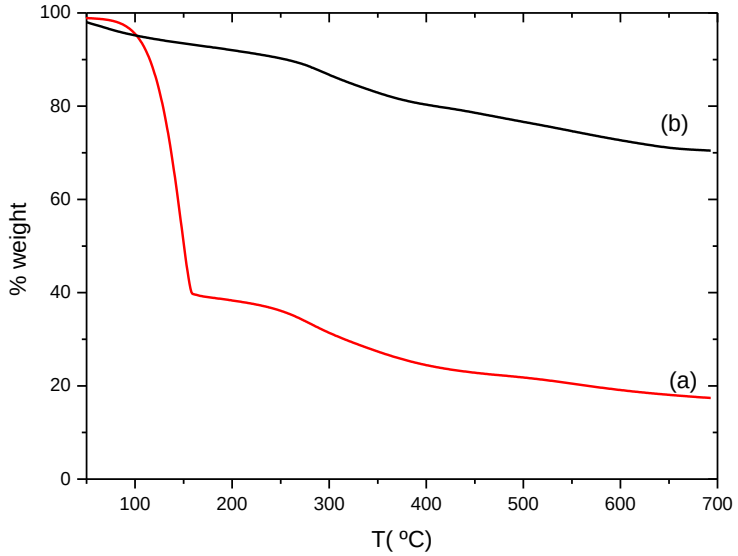

Fig S1- TGA of (a) $Ni(Cp)_2$ and (b) a Ni/SiO_2 SBA-15 sample impregnated with $Ni(Cp)_2$ in $scCO_2$ before reduction